

ABSTRACT

Name: Linda F. Bagby

Department: Physics

Title: Higgs Physics and the Layer Zero Upgrade for D0

Major: Basic Physics

Degree: Master of Science

Approved by:

Date:

Dissertation Director

NORTHERN ILLINOIS UNIVERSITY

ABSTRACT

The origin of the mass of particles is a topic of great interest in the high energy physics community. Electro-weak theory proposes that particles acquire mass by spontaneous symmetry breaking via the Higgs boson. The D0 Collaboration at Fermilab is building a detector, enhancing the ability of the current silicon detector, to study the Higgs mechanism and characterize the Higgs boson. This thesis discusses the Standard Model, Higgs physics, and the new detector, Layer Zero. The motivation to build this detector includes the need to mitigate tracking losses due to radiation damage of the current detector that provides more robust tracking and increases impact parameter resolution. Each of these topics is discussed along with two decay processes of particular interest to Higgs physics. The thesis concludes with a discussion of the ultimate reach for the Higgs boson search with the new detector and the projected luminosity of the Tevatron.

NORTHERN ILLINOIS UNIVERSITY

HIGGS PHYSICS AND THE LAYER ZERO UPGRADE FOR D0

A THESIS SUBMITTED TO THE GRADUATE SCHOOL
IN PARTIAL FULFILLMENT OF THE REQUIREMENTS
FOR THE DEGREE
MASTER OF SCIENCE

DEPARTMENT OF PHYSICS

BY

LINDA F. BAGBY

© Linda F. Bagby

DEKALB, ILLINOIS

MAY 2005

Certification:

In accordance with departmental and Graduate School policies, this thesis is accepted in partial fulfillment of degree requirements.

Thesis Director

Date

ACKNOWLEDGEMENTS

I would like to thank Jack Lockwood for giving me the opportunity to begin my career at Fermilab over 20 years ago, Marvin Johnson for providing guidance to achieve my goals, and Jerry Blazey for his persistent nudging to attend graduate school. In addition, I thank Fermilab for supporting my educational goals. Most of all, I thank my family: my husband for understanding that all meals take ten minutes to prepare and my daughter for helping take notes in Quantum Mechanics class.

DEDICATION

To Gordon, Madison, and the alligator that ate zero

TABLE OF CONTENTS

| | Page |
|---------------------------------------|------|
| LIST OF TABLES | vi |
| LIST OF FIGURES | vii |
| Chapter | |
| 1. INTRODUCTION | 1 |
| 2. STANDARD MODEL | 5 |
| 3. HIGGS PHYSICS | 13 |
| 4. DECAY PROCESSES | 19 |
| 5. LAYER ZERO | 23 |
| Installation and Integration | 30 |
| Low Voltage Power Supply System | 34 |
| 6. CONCLUSION | 37 |
| REFERENCES | 39 |

LIST OF TABLES

| Table | | Page |
|-------|--|------|
| 2.1 | Fermions | 6 |
| 2.2 | Baryons and mesons | 7 |
| 2.3 | Forces of nature and mediating vector bosons | 9 |
| 2.5 | Baryon quark combinations | 11 |
| 5.1 | Layer Zero silicon sensor specifications | 29 |

LIST OF FIGURES

| Figure | Page |
|---|------|
| 1.1. Luminosity threshold for $m_H = 110-130 \text{ GeV}/c^2$ | 3 |
| 2.1. Baryon eightfold way | 10 |
| 3.1. Potential (V) vs Scalar field (ϕ) | 16 |
| 4.1. Feynman diagram for the WH channel decay | 19 |
| 4.2. Feynman diagram for the ZH channel decay | 20 |
| 4.3. Comparison of 95% CL upper limit | 21 |
| 5.1. Run IIa silicon detector | 24 |
| 5.2. Run IIb silicon efficiency degradation | 25 |
| 5.3. Impact parameter resolution | 26 |
| 5.3. South end, looking north, Layer Zero sensor position | 28 |
| 5.4. Run IIa silicon detector with superimposed Layer Zero | 27 |
| 5.5. South end, looking north, Layer Zero sensor position | 28 |
| 5.6. Horseshoe area on the face of the CC | 32 |
| 5.7. Layer Zero adapter card prototype | 33 |
| 5.8. SVX4 isolated power fuse panel | 35 |

CHAPTER 1

INTRODUCTION

The Standard Model is a collection of theories that describe the fundamental constituents of matter and the mechanisms that explain their interactions with the forces of nature. The model describes three fundamental types of particles: leptons, quarks, and force mediators. A special particle related to the mediators, called the Higgs Boson, is of particular interest because the model suggests that it is responsible for imparting mass to particles.

The final signature of an event containing the Higgs particle is similar to many other decay processes. Two channels of interest, due to their relatively low background rates, are $p\bar{p} \rightarrow WH$ (with $W \rightarrow \ell\nu$ and $H \rightarrow b\bar{b}$) and $p\bar{p} \rightarrow ZH$ (with $Z \rightarrow \nu\bar{\nu}$ and $H \rightarrow b\bar{b}$). Extensive study of the two channels has been done by the CDF and D0 collaborations at Fermilab [1,2].

The findings of the sensitivity report show that in the WH channel, with $m_H = 115 \text{ GeV}/c^2$, there will be 2.9 events per fb^{-1} with the production cross-section, the branching ratio (BR), and efficiency folded into the calculation. The largest backgrounds are $Wb\bar{b}$ (108 events) and $t\bar{t}$ (47 events). Other backgrounds, such as $t(W^*)$, WZ , $t(Wg)$, $W + \text{light } q$, and $Wc\bar{c}$, contribute 34 events. After applying a limit

around the m_H window, 2.5 signal events can be expected with 30 background events. After neural network cuts on the $t\bar{t}$ backgrounds are performed, 2.4 signal events will remain with 17 background events.

In the ZH channel, with $m_H = 115 \text{ GeV}/c^2$, 4.3 events per fb^{-1} can be expected after neural network cuts are applied to the top quark event background. Some of these events are due to WH production. Background events due to quantum chromodynamics (QCD), $W/Z b\bar{b}$, and ZZ processes are 61 events per fb^{-1} , 22 events, and 11.5 events, respectively. 19.5 events occur due to other processes. After restricting the m_H window, the estimate reduces to 3.8 signal events and 19.6 background events.

To quantify the sensitivity of finding the Higgs at Fermilab, luminosity thresholds were determined in the study. The thresholds are defined by running pseudoexperiments based on the measured mass distribution (B) and the predicted number of events (A). Two approaches were used, Bayesian [3] and CL_s [4].

The Bayesian approach is based on Bayes's theorem given as

$$P(A|B) = \frac{P(B|A)P(A)}{P(B)} \quad (1.1)$$

This theorem offers a relationship between conditional and marginal probabilities and can be used to update probability distributions with new information from observations. $P(A|B)$ is the posterior probability of A, given new information, B. $P(B|A)$ is the likelihood function for A, given a specific value of B. $P(A)$ is called the prior or marginal probability of A. $P(B)$ is a normalizing constant, representing the prior or marginal probability of B.

The CL_s method is an alternate method of determining the exclusion luminosity threshold. This method utilizes the ratio of the confidences in the signal + background (S + B) to background (B) hypotheses. Poisson counting statistics are used on mass distributions and the associated backgrounds to determine the luminosities in the ratio.

For m_H of 115 GeV/c^2 the thresholds were determined to be 8 fb^{-1} for a 5σ excess (discovery), 3 fb^{-1} for 3σ excess (evidence), and 1.5 fb^{-1} for a 95% confidence level exclusion of the Higgs. Exclusion of m_H up to 130 GeV/c^2 can be attained with an integrated luminosity of 4 fb^{-1} . Figure 1.1 summarizes the luminosity threshold findings, indicated by the narrow curves [1]. The wider curves show luminosity thresholds found by the initial SUSY/Higgs report [5].

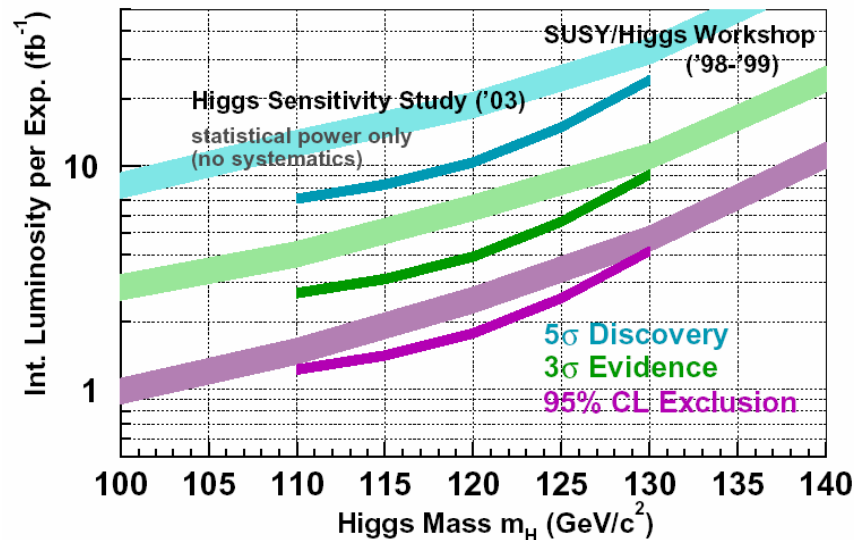


Figure 1.1. Luminosity threshold for $m_H = 110\text{-}130 \text{ GeV}/c^2$.

Since both channels of interest contain bottom quark jets, the ability to tag $b\bar{b}$

events and identify the resulting displaced vertices from the original interaction point is vitally important. A new silicon detector, Layer Zero, is currently being built by the D0 collaboration to provide a means of accomplishing this task. The design of this detector has been optimized to fit within the mechanical constraints of the Run IIa silicon detector and provide increased impact parameter resolution to accommodate greater bottom quark tagging efficiency.

The Standard Model is described in Chapter 2. Chapter 3 gives details regarding Higgs physics. Chapter 4 explores the decay processes of the Higgs. Chapter 5 explains why the new silicon detector, Layer Zero, enhances the opportunity of discovering the Higgs mediator at Fermilab. Chapter 6 offers conclusions of the thesis.

CHAPTER 2

STANDARD MODEL

Now this, O monk, is noble truth that leads to the cessation of pain: this is the noble Eightfold way: namely, right views, right intention, right speech, right action, right living, right effort, right mindfulness, right concentration.

Buddha

Beginning in 1897, with J. J. Thomson's discovery of the electron, scientists have worked to develop a model that describes the fundamental constituents of matter and how the forces of nature influence their behavior. The categorization of the fundamental particles and the theories explaining their behavior are collectively known as the Standard Model.

The Standard model categorizes particles into two main types, fermions and bosons. Fermions, exhibiting $\frac{1}{2}$ integer spin, obey Fermi-Dirac statistics, while bosons, exhibiting integer spin, obey Bose-Einstein statistics. Spin refers to the intrinsic angular momentum of the particle.

Fermions are divided into leptons or quarks. Leptons carrying integer electrical charge are electrons, muons, and taus. Each of the charged leptons has an associated electrically neutral particle known as the neutrino. Quarks carry a fractional electrical charge. Six quarks have been observed in experimentation and are named in order of

increasing mass: up, down, strange, charm, bottom, and top. The top quark was the last quark discovered in 1995 at Fermilab National Accelerator Laboratory by the D0 and CDF experiments.

Table 2.1 shows the fermion particles with their associated charge and mass. Particles existing copiously in nature are Generation I particles. They include two quarks, up and down, along with the electron and its associated neutrino. Generation II particles include the charm and strange quarks along with the muon and muon neutrino. Generation III particles consist of top and bottom quarks as well as the tau with its associated neutrino. Generation II and III particles do not occur readily in nature; therefore, high energy particle accelerators are used to study their properties. Cosmic rays may also be used, but due to the inability to control when they occur, accelerators are preferred.

Table 2.1

Fermions

| Leptons | | | Quarks | | |
|------------|----------------------------|-----------------|--------|----------------------------|-----------------|
| Flavor | Mass (MeV/c ²) | Electric Charge | Flavor | Mass (GeV/c ²) | Electric Charge |
| e | .511 | -1 | u | .0015 - .004 | 2/3 |
| ν_e | < 3 eV | 0 | d | .004 - .008 | -1/3 |
| μ | 106 | -1 | s | .080 - .0130 | -1/3 |
| ν_μ | < .19 | 0 | c | 1.15 - 1.35 | 2/3 |
| τ | 1777 | -1 | b | 4.1 - 4.5 | -1/3 |
| ν_τ | < 18.2 | 0 | t | 178 +/- 4.3 | 2/3 |

Quarks are the constituents of particles called hadrons. Hadrons are subdivided into two types. Mesons are those that are composed of two quarks, a $q\bar{q}$ pair, while baryons are composed of three quarks. Isolated quarks have not been observed. Table 2.2 shows the quark combination of some of the baryons and mesons.

Table 2.2

Baryons and mesons

| Meson | Quark combination | Baryon | Quark Combination |
|-----------------|-------------------|------------------|-------------------|
| π^- pion | $d\bar{u}$ | p proton | uud |
| π^+ pion | $u\bar{d}$ | n neutron | udd |
| K kaon | $d\bar{s}$ | Λ lambda | uds |
| K^- kaon | $s\bar{u}$ | Σ sigma | uds |
| J/ Ψ j/psi | $c\bar{c}$ | Ξ^0 xi | uss |
| Y upsilon | $b\bar{b}$ | Ω^- omega | sss |

Baryons can consist of three of the same quarks. For example, Ω^- is composed of three strange quarks. Since the Pauli Exclusion principle forbids particles to exist in the same state, the sss combination shouldn't exist. To remedy this predicament, a new characteristic was assigned to quarks, color. Quarks are associated with the colors blue, red, or green. Providing that the total color of the baryon is zero or equal amounts of color are present, the combination is acceptable. This rule can be used to explain why isolated quarks and four quark particles are not observed in nature.

It is believed that there are four fundamental forces of nature: Gravitational, Weak, Electromagnetic, and Strong. Each force interacts with specific fundamental

particles of nature, leptons and quarks, via the exchange of a particle known as the force mediator. Physical theories are used to explain each of the forces. Classical, relativistic, and quantum views are represented within these theories.

The gravitational force is classically described by Newton's law of universal gravitation. Einstein's general theory of relativity generalizes this force. A quantum theory describing this force has not adequately been developed and is not included in the Standard Model. The graviton is the mediator of this force. The gravitational force influences all particles.

Weak force interactions are described by a theory initially developed by Fermi. Lee, Yang, Feynman, and Gell-Mann and many others refined Fermi's theory. The mediating particles for the weak force are known as the intermediate vector bosons, $W^{+/-}$ and Z . The weak force interacts with leptons and quarks. Charged lepton and quark interactions are mediated by the $W^{+/-}$ while the Z mediates neutral interactions. The weak force is responsible for nuclear beta decay as well as the decay of pions and muons.

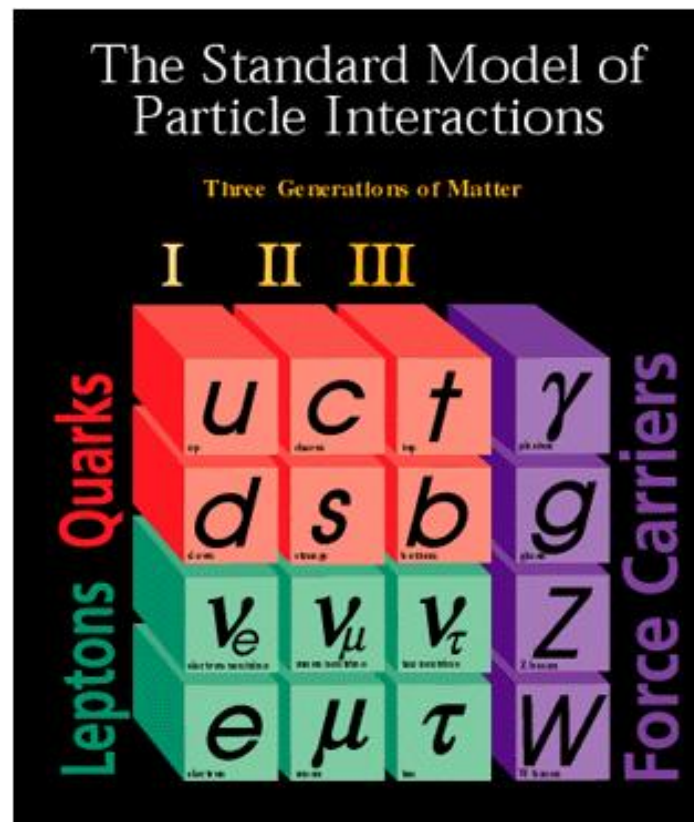
The electromagnetic force is described by electrodynamics theory. Maxwell developed the classical view, consistent with special relativity. During the 1940s, quantum electrodynamics (QED) theory was developed by Tomonaga, Feynman, and Schwinger. The electromagnetic force influences charge carrying leptons such as the electron, muon, and tau via the photon. This force is responsible for the bound state between electrons and nuclei.

Strong force interactions are described by quantum chromodynamics (QCD)

theory. The strong force influences particles that carry color via the gluon mediator. The bound state of protons and neutrons within the nucleus of an atom, as well as the binding of quarks within the proton and neutron, is attributed to the strong force. Table 2.3 summarizes the three generations of matter and the interaction mediators of the four forces of nature.

Table 2.3

Forces of nature and mediating vector bosons



In an attempt to organize the myriad of hadrons discovered, Gell-Mann and Y. Neemann developed the Eightfold Way in 1961 [6]. This method organizes particles, using geometric analogies, based on the particle's quark composition of charmed and strange quarks. This method accurately predicted the existence of the Ω^- baryon and the existence of 6 quarks. Figure 2.1 is a depiction of the Eightfold Way for baryons.

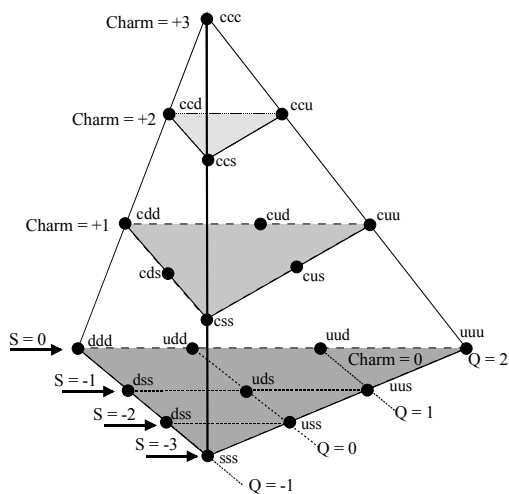


Figure 2.1. Baryon eightfold way.

Each plane corresponds to the charm quantum number. This quantum number represents the number of charm quarks composing the particle. Within the charm = 0 plane, the particles are arranged by strange quantum number, from top to bottom $S = 0$ to $S = -3$. Also within this plane, the diagonal represents the particle's charge beginning with sss , $Q = -1$ to $Q = 2$. Subsequent planes, representing one, two, and three charm

quark baryons, predict the existence of other particles. Table 2.5 summarizes the quark combinations for charmless baryon particles.

Table 2.5

Baryon quark combinations

| Quark Combination | Particle |
|-------------------|-----------------------|
| uuu | Δ^{++} (delta) |
| uud | Δ^+ |
| udd | Δ^0 |
| ddd | Δ^- |
| uus | Σ^{*+} (sigma) |
| uds | Σ^{*0} |
| dds | Σ^{*-} |
| uss | Ξ^{*0} (xi) |
| dss | Ξ^{*-} |
| sss | Ω^- (omega) |

Much like the Eightfold Way provided a mechanism for predicting the existence of particles, flavordynamics theory within the Standard Model predicted the existence of force mediators. Using the idea of treating the Weak and Electromagnetic forces as a single force, the Electro-Weak force, Glashow, Weinberg, and Salam formulated flavordynamics or GWS theory.

GWS theory begins with four massless mediators. As they develop, three of the mediators acquire mass (W^+ , W^- , Z^0), while the photon is massless. A premise of the theory, described in the next chapter, explains that the acquisition of mass is due to the Higgs particle via spontaneous symmetry breaking.

The mass of the W^\pm and Z^0 vector bosons were predicted by this theory to be 82 ± 2 GeV/c² and 92 ± 2 GeV/c², respectively [7]. In 1983 the UA1 and UA2 collaborations at CERN, lead by Carlo Rubbia, announced the discovery of the vector bosons with $M_W^\pm = 81 \pm 5$ GeV/c² and $M_Z^0 = 95 \pm 3$ GeV/c² [8, 9].

CHAPTER 3

HIGGS PHYSICS

The key to Higgs physics begins with the idea of spontaneous symmetry breaking in electro-weak interactions whereby particles acquire mass. It is well known that parity and charge conjugation are not invariant in weak interacting processes. An example of this can be found in the decay process of a pion.

In the $\pi^- \rightarrow \mu^- + \bar{\nu}_\mu$ process, the anti-neutrino has experimentally been measured to be right-handed. Handedness refers to the relative direction of the particle's momentum and spin vectors. Momentum and spin vectors are in the same direction for right-handed particles and oppositely aligned for left-handed particles. Parity invariance applied to the π^- process would indicate that the anti-neutrino would be left-handed, but this state has not been observed in nature. The operation of charge conjugation only changes the sign of the particle quantum numbers. Mass, energy, momentum, and spin remain the same. Applied to the π^- process, the resulting neutrino would be right-handed [7]. Again, there has been no experimental evidence that right-handed neutrinos exist in nature.

Symmetry breaking is the signature of weak interactions. In Electro-Weak theory, the “spontaneous” breaking of these symmetries is associated with Higgs physics. To explain the idea of spontaneous symmetry breaking, we can express the

energy density for a quantum mechanical system using a Lagrangian formalism [10]. Beginning with a Lagrangian's basic premise of $L = T - V$, where T represents the kinetic energy of the particle and V represents the potential energy, an expression for the equations of motion can be developed. From a classical mechanics point of view, the Lagrangian for a system of particles, with generalized coordinates, is expressed as

$$\frac{d}{dt} \left(\frac{dL}{dq_i} \right) - \frac{dL}{dq_i} = 0 \quad (3.1)$$

Applying this equation in terms of a quantum mechanical condition, the time derivative $\frac{d}{dt}$ must be expressed such that it is time invariant. This is accomplished

by using the 4-vector space-time derivative of $\frac{\partial}{\partial x_\mu}$ for $\mu = 1, 2, 3, 4$ or $\frac{\partial}{\partial \mu}$. In

addition to this modification, the discrete coordinate q is replaced with ϕ representing a continuous variable wave or field amplitude. Therefore, the Lagrangian becomes

$$\partial_\mu \left(\frac{\partial L}{\partial (\partial_\mu \phi)} \right) - \frac{\partial L}{\partial \phi} = 0 \quad (3.2)$$

For a free scalar particle with mass μ , the kinetic energy (T) may be represented as

$\frac{1}{2} (\partial_\mu \phi)^2$ and the potential energy (V) can be expressed as $\frac{1}{2} \mu^2 \phi^2$. Therefore,

$$L = \frac{1}{2} (\partial_\mu \phi)^2 - \frac{1}{2} \mu^2 \phi^2 \quad (3.3)$$

Taking the partials of T and V

$$\frac{\partial L}{\partial (\partial_\mu \phi)} = \partial_\mu \phi \quad \frac{\partial L}{\partial \phi} = -\mu^2 \phi \quad (3.4)$$

and substituting into the equation of motion

$$\partial_\mu (\partial_\mu \phi) - (-\mu^2 \phi) = 0 \quad (3.5)$$

we have

$$\partial_\mu^2 \phi + \mu^2 \phi = 0 \quad (3.6)$$

where $\partial_\mu^2 = \frac{\partial^2}{\partial t^2} - \nabla^2$ and $\nabla^2 = \left(\frac{\partial}{\partial x} + \frac{\partial}{\partial y} + \frac{\partial}{\partial z} \right)^2$.

Expanding this relationship to scalar particles interacting with each other, a third term must be added to the Lagrangian of the form $\frac{1}{4} \lambda \phi^4$. λ represents the coupling constant in a four-boson vertex. A fourth order field term is used since odd powers are not invariant under a $\phi \rightarrow -\phi$ transformation and sixth order or higher terms do not comply with renormalization requirements. With this additional term, the Lagrangian becomes

$$L = \frac{1}{2} (\partial_\mu \phi)^2 - \frac{1}{2} \mu^2 \phi^2 - \frac{1}{4} \lambda \phi^4 \quad (3.7)$$

where

$$V = \frac{1}{2} \mu^2 \phi^2 + \frac{1}{4} \lambda \phi^4 \quad (3.8)$$

To realize the minimum value of V , where $\phi = \phi_{\min}$, we take $\frac{\partial V}{\partial \phi}$ and set it equal to 0.

This leads to

$$\frac{\partial V}{\partial \phi} = \mu^2 \phi + \lambda \phi^3 = 0 \quad (3.9)$$

and rearranging terms

$$\phi (\lambda\phi^2 + \mu^2) = 0 \quad (3.10)$$

Setting both terms to 0 we have

$$\phi = 0 \quad \text{and} \quad \lambda\phi^2 + \mu^2 = 0 \quad (3.11)$$

In the first term we see that when $\phi = 0$, $V = 0$. This means that for a massive particle, where $\mu^2 > 0$, the lowest energy vacuum state is when the potential energy is zero. The second term, $\lambda\phi^2 + \mu^2 = 0$, has the solutions

$$\phi = \pm \sqrt{\frac{-\mu^2}{\lambda}} = \pm \nu \quad (3.12)$$

This condition shows that there are two values of the scalar field when the potential is at the lowest energy vacuum state. The minimum scalar field value, when $\mu^2 < 0$, is called the vacuum expectation value, ν . Figure 3.1 is a plot of the potential for $\mu^2 > 0$, representing massive particles, and for $\mu^2 < 0$.

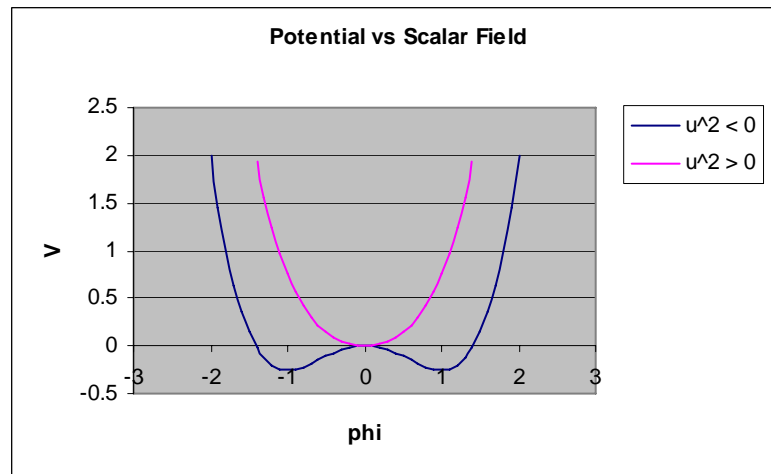


Figure 3.1. Potential (V) vs Scalar field (ϕ).

Evaluating V at $+v$ we find that

$$V = \frac{1}{2} \mu^2 \phi^2 - \frac{1}{4} \lambda \phi^4 \quad (3.13)$$

$$V = \frac{1}{4} \left(\frac{-\mu^4}{\lambda} \right) \quad (3.14)$$

This shows that when the scalar boson field, ϕ , has a value equivalent to the vacuum expectation value, v , the lowest energy state of the potential is a constant value.

Applying this knowledge to weak interactions, we want to investigate small perturbations around the minimum energy value. Adding a perturbation term to the field gives $\phi = v + \sigma$, where σ is a function of x .

Substituting this into the Lagrangian

$$L = \frac{1}{2} (\partial_\mu \phi)^2 - \left(\frac{1}{2} \mu^2 \phi^2 + \frac{1}{4} \lambda \phi^4 \right) \quad (3.15)$$

the kinetic energy, represented by the first term, is expressed as

$$T = \frac{1}{2} (\partial_\mu \sigma)^2 \quad (3.16)$$

Looking at the second term, knowing $\mu^2 = -\lambda v^2$, we see that a mass term appears in the Lagrangian.

$$L = \frac{1}{2} (\partial_\mu \sigma)^2 - \lambda v^2 \sigma^2 - \left(\lambda v \sigma^3 + \frac{1}{4} \lambda \sigma^4 \right) + \text{constant} \quad (3.17)$$

Comparing the second term, in the original Lagrangian, with the second term in the perturbed Lagrangian, we can solve for m , the mass.

$$\frac{1}{2} \mu^2 \phi^2 = \lambda v^2 \sigma^2 \quad (3.18)$$

$$\mu^2 \sigma^2 = 2\lambda v^2 \sigma^2 \quad (3.19)$$

$$\mu^2 = 2\lambda v^2 \quad (3.20)$$

$$\mu = \sqrt{2\lambda v^2} \quad \text{or} \quad m = \sqrt{-2\mu^2} \quad (3.21)$$

This shows that once a perturbation is applied around either of the field minima, $\pm v$, a real mass term emerges. The choice of either $+v$ or $-v$ is arbitrary but once chosen, the symmetry of the system has been broken. This example is referred to as spontaneous symmetry breaking via the Higgs mechanism. Applying this methodology to a complete Lagrangian results in a mass term assignment for the W^\pm and Z^0 vector bosons. In GWS theory, the Higgs is directly coupled to W and Z . In 1979 Sheldon Glashow, Steven Weinberg, and Abdus Salam received the Nobel Prize for their work. The theory was subsequently validated by the 1983 discovery of the W and Z .

CHAPTER 4

DECAY PROCESSES

The Tevatron at Fermilab provides several mechanisms for producing the Higgs boson. Since the Higgs boson is linked to a particle's mass, the most logical place to look for the Higgs would be in decay processes that involve massive particles. W and Z associated production are the best places to find the Higgs, specifically in the channels $p\bar{p} \rightarrow WH$ (with $W \rightarrow \ell\nu$ and $H \rightarrow b\bar{b}$) and $p\bar{p} \rightarrow ZH$ (with $Z \rightarrow \nu\bar{\nu}$ and $H \rightarrow b\bar{b}$).

The first decay process of interest at the Tevatron is the WH channel. Figure 4.1 is the Feynman diagram representing this process. Two quarks from the p-pbar incident beam interact via a virtual W boson, W^* . The W^* decays into a W and a Higgs particle, H. The W then decays into a lepton-neutrino pair while the H decays into a $b\bar{b}$ pair.

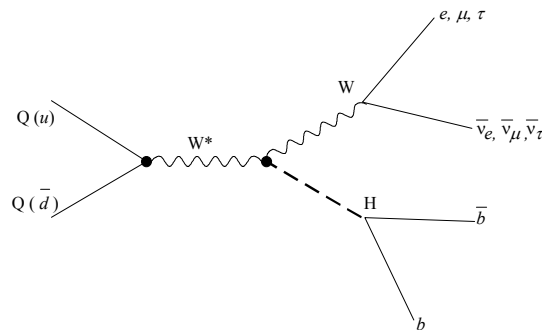


Figure 4.1. Feynman diagram for the WH channel decay.

In a similar fashion the ZH channel is depicted in Figure 4.2. In this case the virtual Z boson, Z^* , decays into a Z and H particle. The Z then decays into a neutrino-anti-neutrino pair while the H decays into the $b\bar{b}$ pair. Although the largest cross-section is in the $gg \rightarrow H$ channel, QCD dominates the backgrounds in the Higgs low mass region ($100 < m_H < 140 \text{ GeV}/c^2$).

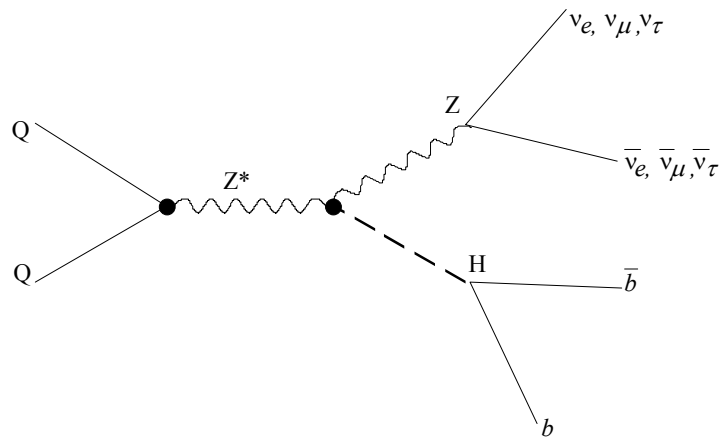


Figure 4.2. Feynman diagram for the ZH channel decay.

The basic procedure used to distinguish signal from background is threefold. First, the event signature is required. For example, in the WH channel, an isolated electron, muon, or track with high transverse momentum accompanied by either a large momentum imbalance or missing transverse energy is required. In addition to this, two or three jets must also be part of the event. Two of the jets must have displaced vertices, indicative of b jets. Next, neural networks are used to eliminate unwanted backgrounds. This method works particularly well removing $t\bar{t}$ background events.

Finally, jets in the remaining events are analyzed to determine the $b\bar{b}$ invariant mass spectrum allowing for the direct reconstruction of the Higgs boson. To increase the sensitivity, both signal and background $b\bar{b}$ events were analyzed in the invariant mass measurement. This method of analysis reduced the required integrated luminosity to measure the Higgs by $\sim 20\%$ as compared to the SUSY/Higgs report which counted events within a mass range.

The latest results in the $Wb\bar{b}$ and WH channel are provided by a paper from the D0 Collaboration [2]. This paper sets the 95% CL (confidence level) upper limit on $Wb\bar{b}$ production of 6.6 pb for $p_T^b > 20$ GeV. In addition, an upper limit is set on WH production of between 9.0 and 12.2 pb, corresponding to a range of mass values for the Higgs boson of 105 to 135 GeV. A previously published report by CDF shows an upper limit for production of ~ 20 pb for $m_H = 120$ GeV [11]. Figure 4.3 compares the findings of D0, previously published results by CDF, and Standard Model expectations.

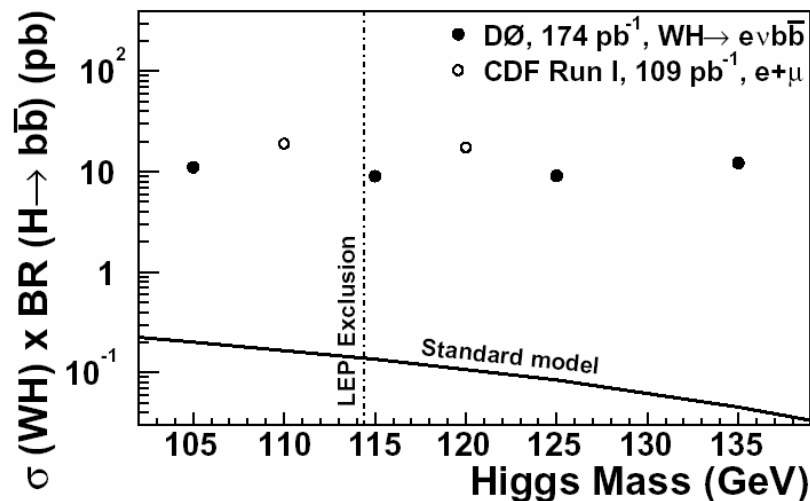


Figure 4.3. Comparison of 95% CL upper limit.

Eleven percent of the systematic uncertainties in the latest results are due to b -tagging efficiency. To minimize these errors a new layer of silicon, mounted closest to the beam pipe, is currently being constructed. The addition of Layer Zero in the D0 experiment will increase b jet sensitivity from $\sim 45\%$ per jet to $\sim 60\%$. Since it is expected that Layer 1 of the Run IIa silicon detector will be damaged by radiation, Layer Zero is vital in the search for the Higgs boson. Details of the Layer Zero detector are described in the next chapter.

CHAPTER 5

LAYER ZERO

If you look at zero you see nothing; but look through it and you will see the world.

Robert Kaplan

The D0 experiment consists of three main types of detector systems. For central tracking, a Silicon Microstrip Tracker (SMT) detector and a Central Fiber Tracker (CFT) are utilized. A two tesla solenoid magnet surrounds the tracking detectors to measure the momentum of charged particles. A full coverage segmented calorimeter, with end calorimeters, measuring energy deposition, surround the central tracking detectors. The calorimeter is surrounded by the muon detector system. The muon detector consists of 1.8 tesla toroids sandwiched between layers of tracking detectors and scintillation trigger counters.

Smaller scale detectors, using scintillating strips, include the Central PreShower (CPS) and forward PreShower (PS). They are located between the Central Calorimeter (CC) cryostat and the End Caps of the Calorimeter (EC). A Forward Proton Detector (FPD) located upstream and downstream of the D0 collision hall, are used to measure high-momentum charged particles with trajectories that are close to the proton and anti-

proton beam directions.

The Run IIa D0 Silicon Tracking detector consist of twelve F-disks positioned between six four-layer barrel structures as shown in Figure 5.1. H-disks units are positioned on both ends of the central structure. The silicon barrels, H-disks, and F-disks were built in the Silicon Detector Facility (SiDet) on the Fermilab site. The detector was installed in 2001 as an upgrade. The origin of the coordinate system, located at the center of the detector, corresponds to a physical location of the Tevatron known as D0. The positive z direction follows the direction of the proton beam. Azimuthal angles increase counterclockwise from $x=0$ as one looks north or “upstream.”

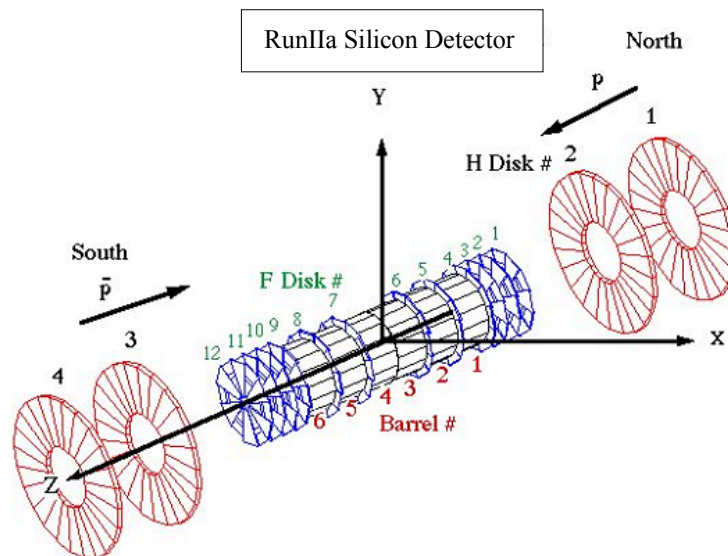


Figure 5.1. Run IIa silicon detector.

The physics motivation to construct Layer Zero is threefold. Compensation for radiation damage of the current detector, increased impact parameter resolution, and enhanced tracking recognition are of paramount importance. Impact parameter resolution is critical in resolving displaced vertices. The tagging of b jets is enhanced with improved tracking recognition.

The Run IIb silicon detector was constructed to withstand approximately 3.5 to 5 fb^{-1} of luminosity before exhibiting radiation damage. It is expected that the inner layer will begin to show radiation damage effects before the end of Run II. Figure 5.2 shows the expected decrease in b -tagging efficiency for various layer failures. For low rapidity events, the efficiency of the detector is 70% if ten percent of the hits are lost in outer layers of the detector indicated in blue. Orange represents a 60% efficiency if 50% of the hits are lost in Layer One and the F-disk detectors. Less than 50% efficiency is expected when Layer One is totally disabled and 50% of the hits in the F-disks are lost.

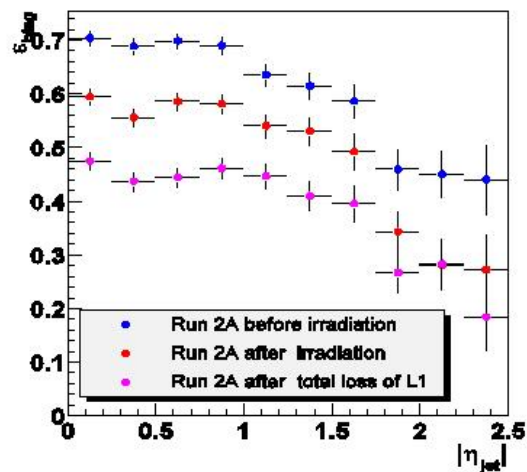


Figure 5.2. Run IIb silicon efficiency degradation.

In addition to increasing efficiency, Layer Zero increases the impact parameter (IP) resolution. Figure 5.3 illustrates the projected resolution for various detector conditions. The plot shows that when Layer One of the current silicon detector is inoperable, the IP resolution will only be about 190 μm for low energy particles. When Layer Zero is installed, the IP resolution improves to 50 μm . The projected resolution curve algorithm was compared to simulation studies and Run IIa data to confirm its validity.

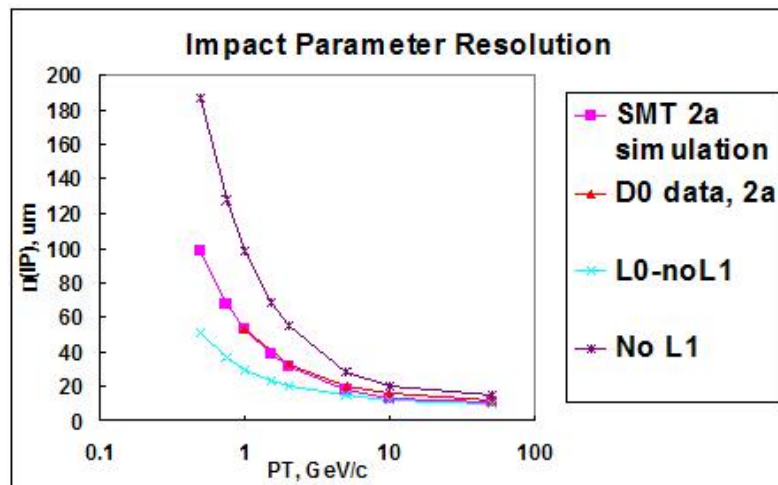


Figure 5.3: Impact parameter resolution.

Figure 5.4 shows an end view, south end looking north, of the Run IIa detector with the new Run IIb Layer Zero superimposed in the center. The color segmentation represents the six Silicon Track Trigger (STT) sectors. Each sector represents 60 degrees starting with sector one in yellow, continuing counterclockwise.

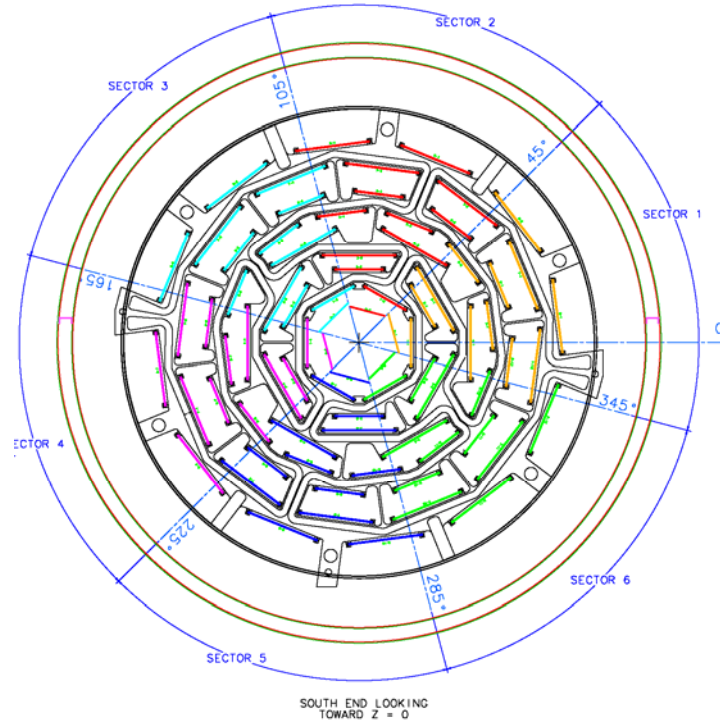


Figure 5.4. Run IIa silicon detector with superimposed Layer Zero.

The new inner layer silicon detector, Layer Zero, is designed to fit inside the existing Run IIa detector and will utilize much of the existing infrastructure as well as the new electronics and readout designed for the cancelled Run IIb silicon replacement. The detector must be able to slide over a beam pipe and associated mounting flanges that have a diameter of 30.48 mm. It is also required to maintain an approximate 1 mm separation from the beam pipe to limit capacitive noise pickup. Layer Zero must clear the innermost layer of the current detector constraining the overall diameter to 44.04 mm. Given the tight mechanical constraints, the detector is designed to maximize acceptance (98.5%) and readout segmentation. Figure 5.5 shows the sensor orientation.

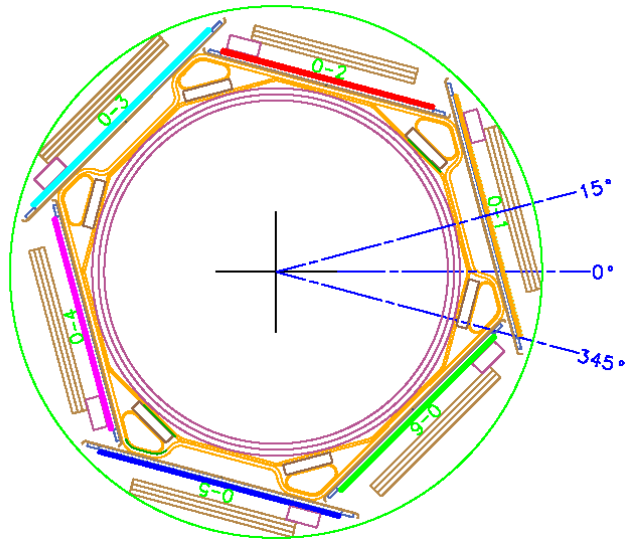


Figure 5.5. South end, looking north, Layer Zero sensor position.
(Overall diameter is approximately 44 mm.)

Layer Zero is composed of 48 silicon sensors manufactured by Hamamatsu. Z segmentation is limited to eight sensors of 70 and 120 mm lengths because of the radial buildup of the cable bundles. This arrangement provides better segmentation near $Z=0$ and equalizes the load capacitance by having lower sensor capacitance on the chains using the longest analog cables. Inner radius positions utilize 71 μm pitch sensors while 81 μm pitch sensors are used at larger radius positions. A single cable pitch is realized by utilizing pitch adapters mounted on the sensors that also carry decoupling capacitors. Table 5.1 summarizes the Layer Zero detector specifications. Each parameter is defined with respect to the Z location. Each end of the detector, north and south, is built with Z1 corresponding to the z location closest to the interaction point for a total of 8 sensors per sector.

Table 5.1

Layer Zero silicon sensor specifications

| | Z1 | Z2 | Z3 | Z4 |
|--------------------------|--------|--------|--------|--------|
| Detector length (mm) | 70 | 70 | 120 | 120 |
| Strip Pitch (microns) | 71 | 71 | 81 | 81 |
| Active width (mm) | 18. 18 | 18. 18 | 20. 74 | 20. 74 |
| Radius (inner, mm) | 16. 10 | 17. 60 | 16. 10 | 17. 60 |
| Max. angle (radians) | . 51 | . 48 | . 57 | . 53 |
| Analog cable length (mm) | 343 | 317 | 241 | 165 |
| Total Capacitance (pf) | 20. 4 | 19. 5 | 22. 8 | 20. 2 |
| Total Noise (electrons) | 1419 | 1378 | 1528 | 1407 |
| S/N (normal incidence) | 16. 2 | 16. 7 | 15. 1 | 16. 3 |
| S/N (edge) | 7. 3 | 8. 1 | 7. 0 | 8. 2 |

Hybrids are located outside of the active volume region and are connected to the sensors with fine pitch analog cables. The analog cable lengths, manufactured by Dyconex, vary with the longest at 343 mm, and have a capacitance of 0.35 pF/cm. Each BeO ceramic hybrid holds two SVX4 chips. The SVX4 chip is a 0.25 μm silicon readout chip originally developed for the Run IIb upgrades. These chips use a protocol similar to the currently installed SVX2 chips but operate with a single 2.5 V supply rather than the 3.3 V and 5 V supplies needed for the SVX2.

A number of Run IIb studies have established that low coherent noise can be achieved by good low inductance ground connections to the support structure. This is accomplished by co-curing mesh ground planes onto the carbon fiber support structure and utilizing low inductance flex circuits which carry bias and ground from the bottom to the top of the sensors. Grounding of the SVX4 reference to the support structure is accomplished with vias that are plated through the hybrid to contacts on the co-cured

flex circuit. The signal/noise is roughly equal at each Z location with adequate signal available for tracks incident at the extreme edges of the detector for reliable readout and reconstruction.

Digital signals from the hybrid are brought to a junction card mounted off of the Run IIb silicon support structure using a kapton flex digital jumper cable, DJC. The junction card provides a means of coupling the DJC to a twisted pair cable that is then interfaced to the existing readout system using active circuitry on an adapter card mounted on the wall of the D0 calorimeter.

The support structure of Layer Zero is a continuous conductor between the North and South ends of the detector. Due to this construction, the potential exists for a ground loop encircling the D0 calorimeter. To minimize ground loops and provide 2.5 V power, required by the SVX4 readout chip, an Adapter Card (AC) and Low Voltage Power Supply system has been designed to isolate the Layer Zero detector from the currently installed detector electronics. The isolation requirement between the data acquisition system and the SVX4 reference is at least 10 Ohms.

Installation and Integration

As a member of the Run IIb Layer Zero Detector Upgrade project, I oversee the installation and integration of the detector into the experiment insuring as smooth a

transition as possible. I have identified several problems and formulated solutions to accomplish this task.

The first design constraint was to realize how the new detector would be read out within the data acquisition system. There are 912 data acquisition chains, mapped into 456 readout channels, in the system with virtually no space available to add more to accommodate the new detector. After reviewing the state of the current detector, it was suggested that the outer H-disk detectors be removed to accommodate the 48 channels required by Layer Zero. Removing the two outer H-disks freed up 96 readout channels, twice as many as required. The abundance of free channels appeared to be quite adequate until I realized the next constraint.

The second constraint is imposed by the Silicon Track Trigger (STT) system. The data acquisition system consists of Adapter Cards (AC), Interface Boards (IB), Sequencers (SEQ), and VME Readout Buffer boards (VRB). The AC is used to convert single-ended SVX4 control signals from the IB to differential signals, provide isolated power regulation to the SVX4, and generate an extra control signal required by the readout chip. The IB is used to monitor bias currents and voltages. Silicon sensor bias voltage is interfaced between the high voltage system and the AC via the IB as well as SVX4 control signals from the SEQ. The SEQ is used to generate control signals, used by the SVX4, and insures readout synchronization with the experiment's trigger framework. The VRB cards provide a bank of buffers used to store data acquired by the readout chip.

The Run IIa detector is divided into six sectors to accommodate the requirements of the STT system. The AC card positions correspond to a specific sector. Figure 5.6 is a graphic of the “horseshoe” area where the ACs are located. The narrow cables are low mass flexible circuits. The wider cables, dressed along the face of the EC, are the 80 conductor cables. Figure 5.7 shows the installation of the new Layer Zero prototype Adapter Card on the horseshoe. Positions 16 and 17 were chosen, which map into STT sector 3 on the northwest side of the detector. One can see how important it is to insure dimensional correctness of the AC. If the card is too wide it will interfere with adjacent Run IIa cards. If it’s too long, 80 conductor cables will have to be adjusted.

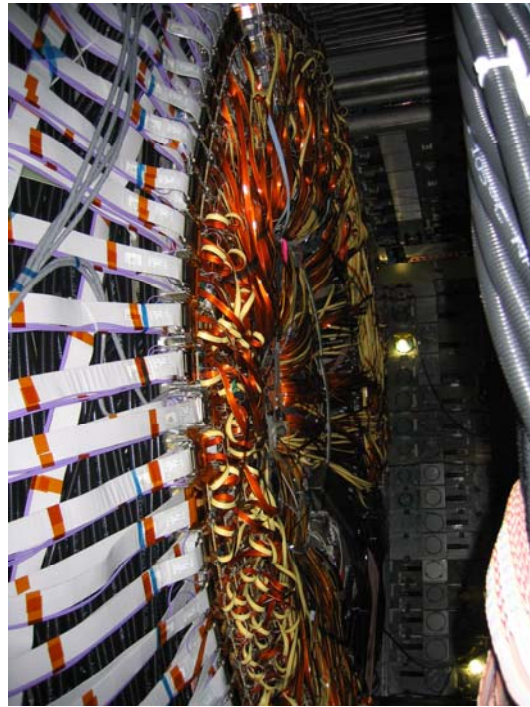


Figure 5.6. Horseshoe area on the face of the CC.

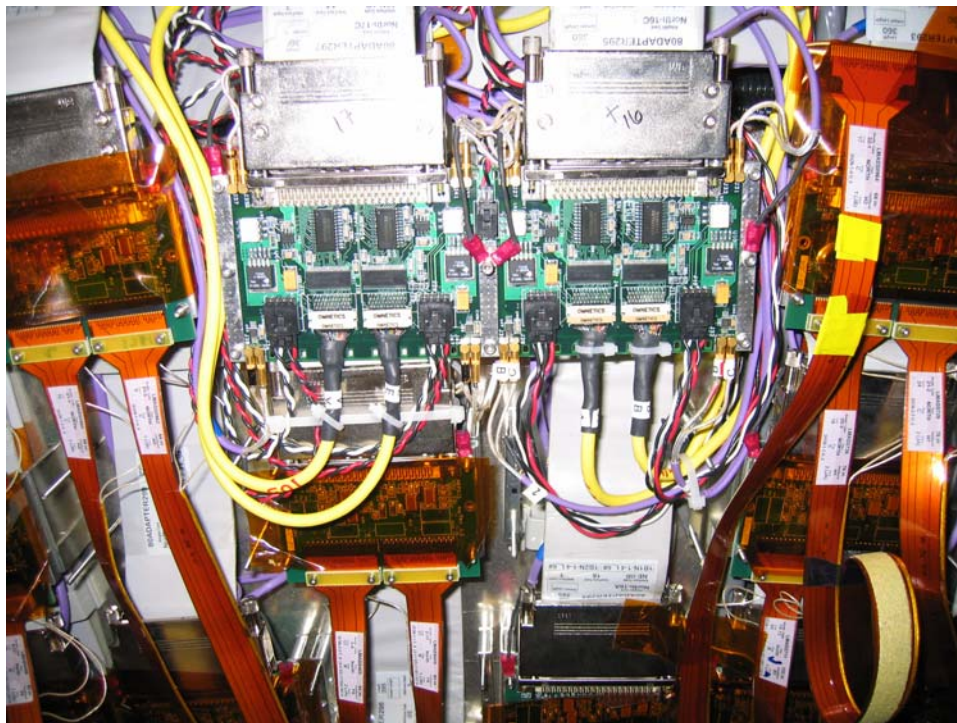


Figure 5.7. Layer Zero adapter card prototype.

To insure that the cabling from each sector specific Layer Zero detector would reach the corresponding sector specific AC location, the length of the cable was specified. The new AC card dimensions were also specified to minimize the need to disturb installed 80 conductor cables. So now we have a design that accommodates any AC position. It appears that since we know which AC positions to use and that the cables will reach, we have established a smooth installation. However, an additional constraint was discovered.

The third constraint is that each AC accommodates two detector chains, read out on one cable connected to the IB and subsequently to a SEQ board. Unfortunately, an

Inner H-disk chain was matched with an Outer H-disk chain on each AC for the Run IIa detector. By removing the Outer H-disk chain, a free chain input is provided but it's matched with an SVX2 Inner H-disk chain. This is a problem due to the operation of the SEQ and the fact that Layer Zero utilizes SVX4 readout chips.

The SEQ provides the proper control signals to a SVX readout chip. Luckily, the SEQ is divided in half such that the same board with a relatively simple firmware modification can generate different control protocols. This means that the SVX4 chains of Layer Zero must not only be mapped to one cable coming from the AC, but at the same time it is desirable to have them map into either the top or bottom half of a SEQ board. By only utilizing half of a SEQ board for Layer Zero, the experiment has the flexibility of using the other half for either SVX2 or SVX4 readout chains. To meet the SEQ constraint, half of the Inner H-disk low mass cables must be moved to AC locations already instrumented with an Inner H-disk.

A map was generated to accomplish the required cable moves. One quarter of the moves were tried during the 2004 shutdown. Unfortunately we had limited success due to the length of the low mass cables and the number of bad readout channels, assumed to be repairable. However, we were able to move enough cables to accommodate the installation of four Layer Zero prototype readout chains.

Low Voltage Power Supply System

In addition to the mapping work, I am responsible for the design and installation of the Low Voltage Power Supply System for Layer Zero. Due to the desire to

minimize possible noise interference of Layer Zero into the existing detector and insure the integrity of the readout, the group decided to use an isolated power supply system to bias the SVX4 and the control signal drivers.

A Vicor power supply system provides power to the IB and SVX2, via the 80-conductor cable, in the current experiment. This system will be retained to provide power to the IB and portions of the AC electronics. Based on previous Run IIB silicon upgrade design work, the isolated system uses a commercial Wiener supply to provide power to the SVX4. The final power supply system was installed during the shutdown previously mentioned. It is composed of the Wiener mainframe housing, four power supply modules including a spare for each of the four detector quadrants, an Interlock chassis, and dedicated fuse panel. Figure 5.8 is a photograph of the fuse panel installed on the west side of the experiment. An identical panel is installed on the east side. The supply is interfaced with the interlock system used to monitor the temperature of the silicon and the D0 fire system.

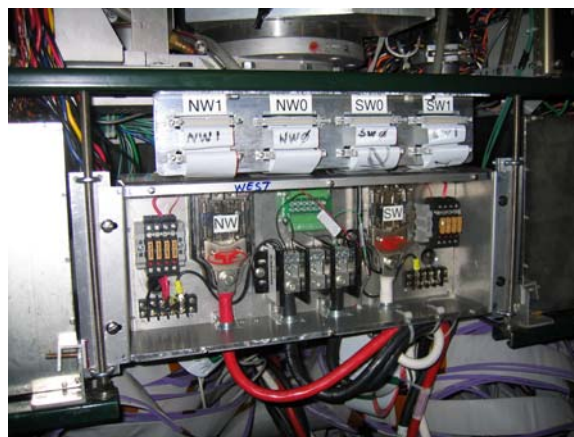


Figure 5.8. SVX4 isolated power fuse panel.

The Wiener supply uses CAN bus protocol as the slow control system. Rather than have a dedicated PC to monitor the supply, I spearheaded an effort to incorporate the system into the experiment's EPICS system. To do this, the CAN bus protocol needed to be converted into VME protocol such that a Power PC Controller (PPC), already part of the slow control system at D0, could communicate with the device. A converter daughter card was purchased for use on the PPC and the software is currently being developed by the D0 Controls group. An added feature of this effort is that when the software is complete, any CAN bus device can be instrumented into the EPICS system.

CHAPTER 6

CONCLUSION

This thesis began with a look at the sensitivity of the Tevatron for finding the Higgs boson. Background information on the Standard Model was provided to give context for the importance of the Higgs. The chapter on Higgs physics illustrates the concept of spontaneous symmetry breaking. Decay processes in which the Higgs can be found and the latest results from D0 are discussed. Finally, the design specifications of a new detector, Layer Zero, are presented with my specific responsibilities to the project.

The projected luminosity, delivered by the Tevatron, during the Run IIb run is 8 fb^{-1} [11]. The ultimate reach for the Higgs search is given in Figure 1.1 [1]. If the integrated luminosity during Run IIb reaches 8 fb^{-1} , the plot indicates that a signal from Higgs, up to a mass value of $128 \text{ GeV}/c^2$, will be seen with adequate statistics to indicate evidence of existence. If the mass of the Higgs is around $115 \text{ GeV}/c^2$, with the same amount of integrated luminosity, discovery can be claimed.

The integrated luminosity tolerance of the Run IIa silicon detector is $2\text{-}4 \text{ fb}^{-1}$ [12]. Once this luminosity is reached, radiation damage to the inner layers of the detector will greatly deteriorate our ability to efficiently tag b jets, thus compromising the search for the Higgs boson. The addition of the Layer Zero detector compensates for this radiation damage in addition to improving pattern recognition and increasing

impact parameter resolution. The Layer Zero project is on schedule and will be installed during the 2005 shutdown at Fermilab.

REFERENCES

- [1] CDF and D0 Collaboration, *Results of the Tevatron Higgs Sensitivity Study* (FERMILAB-PUB-03/320-E, 2003).
- [2] V. Abazov *et al.* (D0 Collaboration), submitted to Phys. Rev. Lett., *A Search for $Wb\bar{b}$ and WH Production in $p\bar{p}$ Collisions at $\sqrt{s} = 1.96$ TeV* (FERMILAB-PUB-04/288-E, 2005).
- [3] Bayes' Theorem [On-line report] retrieved December 16, 2004:
http://en.wikipedia.org/wiki/Bayesian_inference.
- [4] A. L. Read, *Modified Frequentist Analysis of Search Results (The CL_s Method)* in *Proceedings of the 1st Workshop on Confidence Limits* (CERN Yellow Report CERN 2000-005 Geneva: Switzerland, 2000).
- [5] M. Carena, J. S. Conway, H. E. Haber, and J. D Hobbs, *et al.*, “*Report of the Higgs Working Group of the Tevatron Run 2 SUSY/Higgs Workshop*,” hep-ph/0010338 (2000).
- [6] R. A. Wehr, *Physics of the Atom* (Addison-Wesley: Massachusetts, 1984).
- [7] D. Griffiths, *Introduction To Elementary Particles* (John Wiley & Sons: New York, 1987).
- [8] G. Arnison *et al.* (UA1 Collaboration), Phys. Lett. **126B**, 398, (1983).
- [9] M. Banner *et al.* (UA2 Collaboration), Phys. Lett. **122B**, 476, (1983).
- [10] D. H. Perkins, *Introduction to High Energy Physics* (Cambridge University: Cambridge, England, 2000).
- [11] F. Abe *et al.*, Phys. Rev. Lett. **82**, 2038, (1999).
- [12] D0 Collaboration, *D0 Layer 0 Conceptual Design Report DRAFT Version 2.5* [On-line report] retrieved September, 2004: http://d0server1.fnal.gov/projects/run2b/Silicon/www/smt2b/Layer00/D0_L0_CDR_v2.5.doc, (2003).